frontiers | Frontiers in Nuclear Engineering

TYPE Original Research
PUBLISHED 05 January 2026
DOI 10.3389/fnuen.2025.1729916

OPEN ACCESS

EDITED BY
Tao Wu,
Huzhou University, China

REVIEWED BY
Dominik Zbinden,
ETH Zurich, Switzerland
Clare Thorpe,
The University of Sheffield, United Kingdom

*CORRESPONDENCE
Stefan Finsterle,
stefan@finsterle-geoconsulting.com

RECEIVED 22 October 2025
REVISED 27 November 2025
ACCEPTED 28 November 2025
PUBLISHED 05 January 2026

CITATION
Finsterle S, McLachlan JR, Hannon MJ Jr., Sloane J, Abergel RJ and Peterson PF (2026) Modeling glass degradation and release of radionuclides from vitrified waste for performance assessment simulations. *Front. Nucl. Eng.* 4:1729916. doi: 10.3389/fnuen.2025.1729916

Modeling glass degradation and release of radionuclides from vitrified waste for performance assessment simulations

Stefan Finsterle[1]*, Jeffrey R. McLachlan[2], Michael J. Hannon Jr.[3], Jesse Sloane[4], Rebecca J. Abergel[2] and Per F. Peterson[2]

[1]Finsterle GeoConsulting, LLC, Kensington, CA, United States, [2]Department of Nuclear Engineering, University of California, Berkeley, Berkeley, CA, United States, [3]Hannon Clean Energy, LLC, Bloomington, IN, United States, [4]Deep Isolation Nuclear, Inc., Berkeley, CA, United States

The release of radionuclides initially encapsulated in a slowly degrading solid waste form and contained in an eventually corroding canister defines the source term for numerical simulations for the assessment of a geologic repository for high-level radioactive waste. While the details of waste degradation, canister corrosion, and dissolution and mobilization of the radionuclides in pore water include complex chemical reaction and transport processes that are coupled to the thermal, hydrological, microbiological, and mechanical conditions in the repository, the source-term model suitable for use in a numerical performance assessment model should be a defensible abstraction of these mechanisms. We developed a radiological source-term model and implemented it into a non-isothermal flow and transport simulator. While the proposed source-term model is applicable to various waste forms, canister systems, and disposal concepts, we specifically considered radionuclide releases from vitrified high-level waste placed in a cylindrical canister disposed in a deep vertical borehole repository. In this model, waste degradation is a function of temperature, and it can be adjusted to evaluate the influence of and propagate uncertainties in pH, passivation reactions, and chemical conditions as well as geometrical factors. The time-dependent, congruent release of safety-relevant radionuclides present in the decaying inventory is then calculated. Finally, the radionuclides are mobilized by diffusive and advective transport according to the thermo-hydraulic conditions prevailing in the near field of the repository, from where they migrate through the geosphere to the accessible environment. We examine the influence of the source-term model's parameters on performance assessment calculations through sensitivity and uncertainty propagation analyses, identifying influential factors and confirming the upper bound of their impact. These considerations align with the overarching goal of repository design, which is to demonstrate that engineered and natural barriers can collectively delay radionuclide migration for timescales far exceeding human planning, thereby providing multiple, redundant barriers against environmental contamination.

KEYWORDS

iTOUGH2, performance assessment model, radioactive waste disposal, radionuclide source-term model, vitrified waste, waste degradation

1 Introduction

The premise of geologic disposal of radioactive waste is to isolate the waste from humans and the environment by relying on a multi-barrier system that protects, immobilizes, and confines the waste in the repository. Nevertheless, it is anticipated that radionuclides will eventually escape the confinement of the disposal canister and be released into the near field, from where they slowly migrate towards the land surface (IAEA, 2011; SKB, 2011; Nagra, 2014a; NRC, 2014; Andra, 2016). The details of contaminant transport within the geosphere are of great significance as they determine the delay of the arrival of the radionuclides in the accessible environment, allowing them to decay to acceptably low levels that are compliant with an applicable dose standard.

The source of radionuclides migrating through the natural barrier system is given by the rate and timing with which they are released from the canisters. The canisters are part of the engineered barrier system (EBS), which also includes the solid waste form, a potential bentonite buffer, liners or casings, as well as various plugs that seal the disposal section of the repository from the access structures. In what follows, we define the source term as the time-dependent release rate of radionuclides from the canister, allowing the use of these rates in a variety of repository concepts (mined as well as deep horizontal or vertical borehole repositories) irrespective of the details of the EBS design or the scale and scope of the transport model. For example, the source term can be used as part of a submodel that details the coupled processes within the buffer and near field during the early times after waste emplacement. Alternatively, it can be used in a repository-scale model that focuses on simulating long-term radionuclide transport for various nominal and disruptive scenarios or bounding calculations.

Because the chemical and mechanical evolution of the near field cannot be represented mechanistically in a large-scale repository model, the development of a source-term framework becomes a critical step in linking experimental observations with performance metrics. The radiological source-term model proposed here is specifically developed for integration in a comprehensive post-closure performance assessment (PA) model, where all safety-relevant components of both the engineered and natural barrier systems as well as the main hydro-geological features and key flow and transport processes are included in a single model. Such a comprehensive model can be used for screening calculations and sensitivity analyses, preliminary assessments of repository safety, evaluations of barrier performance, and eventually total system performance simulations. The main advantage of using a fully integrated PA model is that the changes in any model parameter and its uncertainty can be propagated through each system component to examine its impact on ultimate performance metrics, such as peak exposure dose. In particular, the relative importance of the source-term model can be examined, guiding the efforts that need to be placed on the accuracy with which each of its parameters must be determined. This approach also inherently accounts for feedback mechanisms between the components of the repository system without the need to transfer information among various submodels with different levels of abstraction, which is conceptually challenging and often not transparent. An example of such a comprehensive PA model in the context of waste disposal in a deep borehole repository (Muller et al., 2019) is described in Finsterle et al. (2020), Finsterle et al. (2021a), and Finsterle et al. (2021b).

While canister corrosion and waste-form degradation are innately chemical and mass-transport processes (Curti et al., 2006; Cassingham et al., 2015; Gin et al., 2017; Kienzler et al., 2012; Thorpe et al., 2021; Curti, 2022), the large-scale post-closure PA model for the prediction of radiological consequences in the biosphere typically focuses on thermal and hydrological processes that affect radionuclide transport and their retardation (specifically sorption and matrix diffusion). Therefore, the source-term model includes thermal and hydrological interactions between the waste form and the near field (Muñoz et al., 2024); however, chemical processes are not mechanistically simulated, but replaced by approximations and the choice of appropriate effective parameters. In particular, it is assumed that the main effect of canister corrosion on radionuclide release is the time when the canister is breached. At this instance, water enters the canister, initiating the degradation of the waste form. Diffusive and advective releases of radionuclides through the breached canister shell or its corrosion products is thus approximated by a time-dependent increase in the canister's permeability, porosity, and other thermal-hydrological properties, including the sorption coefficient. The lifetime of the canister system (which may include multiple containers within a single canister) can be parameterized and adjusted to investigate its importance for long-term repository performance. Note that the generation of corrosion gases (both on the inside and outside surfaces of the canister) can be included in the source-term model (Finsterle et al., 2025), affecting pressure conditions that drive advective transport and the mobilization of volatile radionuclides. Note that dissolved hydrogen gas may suppress the degradation of some waste forms (SKB, 2005).

Similarly, the waste degradation model proposed here does not explicitly simulate glass dissolution and glass alteration reactions but is based on measurements of the surface degradation rate, which is adjusted for thermal and chemical conditions in the waste form if they deviate from a reference state (McLachlan et al., 2024). The evolving surface alteration rate is applied to the slowly reducing size of the cylindrical waste form to yield the rate with which the waste matrix dissolves. This in turn determines the congruent dissolution of radionuclides into the surrounding pore water. Thus mobilized, the radionuclides are transported away from the canister into the near field and geosphere.

Finally, the radionuclides contained in the waste form emit radiation that deposits energy mainly into the waste form and canister and heats the near field of the repository. The temperature increase resulting from this heat source affects degradation rates and diffusion coefficients. Moreover, it leads to the expansion of the pore water and solid materials, which enhances the driving forces (i.e., pressurization) for advective transport. Sufficient heating may induce boiling, which exacerbates this effect.

The overall goal of the work presented here is to introduce a radionuclide source-term model tailored for integration into a thermal-hydrological PA model that can be used to directly evaluate the impact of uncertainties in source parameters on peak exposure dose and other performance metrics. The scope of this paper is limited to introducing the source-term model, with

effective parameters derived from alteration-rate measurements of vitrified high-level radioactive waste. The application of the source-term model is demonstrated in the context of a sensitivity and uncertainty propagation analysis, using an integrated PA model of a vertical borehole repository.

2 Materials and methods

The following subsection describes the source-term model, which includes the factors affecting waste degradation and radionuclide release. The post-closure PA model described in Section 2.2 contains the proposed source-term model and is used to evaluate the impact of the source-term model parameters on peak dose. The source-related parameters to be used for the demonstration of the model are summarized in Section 2.3.

2.1 Waste degradation model and radionuclide release

After canister breach, the radionuclide inventory initially encapsulated in the waste form and contained in the canister is slowly released by the degradation of the waste form. The degradation of various waste forms, specifically spent nuclear fuel and amorphous waste forms such as vitrified, metallic, ceramic, and frozen halide salt waste forms, has been extensively studied theoretically, experimentally, numerically, and using natural analogues (Harper et al., 2024; Muñoz et al., 2024; McCloy et al., 2024; Deissmann et al., 2025; Marcial et al., 2025). This extensive body of work forms the empirical and theoretical foundation for the source term in PA models, offering rate constants, activation energies, and mechanistic insights that enable extrapolation over the geologic timescales relevant to repository safety. Focusing on vitrified waste, the dissolution and alteration of the glass matrix is recognized as a complex physicochemical process that includes several stages with changing degradation rates that depend on the glass composition, temperature, solution chemistry, self-irradiation, exposed surface area, and other factors (Gin et al., 2017; Curti, 2022). Furthermore, as the network of glass-forming oxide dissolves, the radionuclides are released either congruently or incongruently, i.e., radionuclides are released either faster or slower than the glass constituents. Different mechanisms with similar complexities arise in the degradation of spent nuclear fuel and other waste forms, as described in detail in, e.g., Thorpe et al. (2021), Curti (2022), and Nagra (2024) as well as the references cited in Table 3 below.

For application in a PA model, these complexities are typically simplified to different levels of abstraction, with uncertainties handled by the choice of effective parameters and conservative assumptions. The waste degradation and radionuclide release model described below attempts to capture the main factors and processes that affect the source term and to directly integrate them into a PA model.

The mass of radionuclides present in the waste form changes with time because of (a) radioactive decay and ingrowth, and (b) radionuclide release from the degrading waste form. Radioactive decay of the inventory encapsulated in the waste form—and, if it is a member of a decay chain, its potential generation by the decay of the parent radionuclide—is described by Equation 1:

$$m(t) = m_0 \cdot e^{-\lambda t} + m_p(0)\frac{\lambda_p}{\lambda - \lambda_p}\left(e^{-\lambda_p t} - e^{-\lambda t}\right) \tag{1}$$

where $m_0 = m(0)$ (kg) is the initial radionuclide mass (referred to as inventory), $\lambda = \ln(2)/t_{1/2}$ (s^{-1}) is the decay constant, $t_{1/2}$ (s) is the radionuclide's half-life, and t is the elapsed time since the reference time, i.e., the time the inventory was determined. Note that the decay of a parent radionuclide (indicated by subscript $()_p$ in Equation 1) may increase the mass of a radioactive daughter product, which also needs to be tracked in the model, both within the waste form and in the geosphere. A relevant example is the ingrowth of ^{241}Am caused by the decay of ^{241}Pu. The production of short-lived daughter products is typically directly included in the dose conversion factor. The decay equation applies to radionuclides that are encapsulated in the solid waste matrix, dissolved in the pore fluid within the canister, or migrating through the engineered and natural barrier systems.

In addition to radioactive decay, the mass of radionuclides in the waste form declines as the waste form degrades and isotopes are released from the solid matrix. It is assumed here that the radionuclides are distributed homogeneously within the waste form, and that they are mobilized proportional to the rate with which the waste form dissolves; this is referred to as a congruent release of radionuclides. This assumption is generally conservative for vitrified wastes, because data indicate high retention for all nuclides in the glass alteration layer (Curti et al., 2006). Moreover, for sufficiently high degradation rates and limited removal of radionuclides away from the canister by diffusion and advection, the released radionuclides may reach their solubility limit in the water. This can be approximately simulated by assuming precipitation or sorption of radionuclides within the canister.

The waste degradation rate is typically described as a fraction of the remaining waste mass ω (s^{-1}) or by a specific degradation rate q_0 (kg m^{-2} s^{-1}) acting on the exposed surfaces of the waste form. These normalized degradation rates q may be assumed constant in time or dependent on temperature and other factors (such as pH or an affinity term). The dependence of the degradation rate on temperature is described by the Arrhenius equation combined with adjustment factors to account for pH and other chemical, radiological, and geometrical impacts (see, e.g., Cassingham et al., 2015; Thorpe et al., 2021; Kienzler et al., 2012):

$$q(T,t) = \Upsilon_{\mathrm{pH}} \cdot \Upsilon_{\mathrm{SA}} \cdot \Upsilon_{\alpha} \cdot \Upsilon_{\mathrm{L}} \cdot \Upsilon_{\mathrm{Si}}(t) \cdot q_0 \cdot \exp\left[\frac{-E_a}{R} \cdot \left(\frac{1}{T(t)} - \frac{1}{T_0}\right)\right] \tag{2}$$

In Equation 2, T (K) is temperature, q_0 (kg m^{-2} s^{-1}) is the rate constant at reference temperature T_0 (K), E_a (J mol^{-1}) is the activation energy, and R (J K^{-1} mol^{-1}) is the universal gas constant. The dimensionless factors Υ_i can be used to account for other effects, such as:

- Υ_{pH}: pH dependence with respect to neutral water, $\Upsilon_{\mathrm{pH}} = 10^{|\eta \cdot (pH-7)|}$
- Υ_{SA}: Surface area factor to account for fracturing of the waste form

- Υ_α: Impact of excessive alpha radiation on waste degradation rate
- Υ_{Si}: Affinity term; $\Upsilon_i = (1 - Q/K)$, where Q is activity and K is the equilibrium constant. Species i is typically selected as $Si(OH)_4$ for borosilicate glass waste forms. However, different species may limit the degradation of other waste forms. In particular, aluminoborosilicate glasses may be affected by both the concentration of $Si(OH)_4$ and $Al(OH)_3$ in the leachate, or by multi-element minerals, suggesting that the affinity term may need to include additional species; see Fournier et al. (2018) and references therein. As geochemical reactions are not tracked, the impact of orthosilicic acid on waste degradation rate is implemented using a parameterized function that reduces the rate after the canister breach time t_b, approaching the residual rate $q_r = q_o \cdot \Upsilon_r$ using an exponential decay model or reaching it at time t_e when affinity effects cease through a smooth interpolation function:

Exponential decay model (Equation 3)

$$\Upsilon_{Si}(t) = \Upsilon_r + (1 - \Upsilon_r) \cdot e^{-\lambda \cdot (t - t_b)} \tag{3}$$

Smoothstep model (Equation 4)

$$\Upsilon_{Si}(t) = \Upsilon_r + (1 - \Upsilon_r) \cdot \left(k^2 \cdot (3 - 2k)\right) \tag{4}$$

where k is defined by Equation 5:

$$k = 1 - \left(\frac{t - t_b}{t_e - t_b}\right) \quad \text{for} \quad t_b < t < t_e \tag{5}$$

Potential rate resumption (Fournier et al., 2014) is currently not implemented in the model (see related discussion in Section 3.2).

- Υ_{CCL} Impact of chemical composition of the leachate (including salinity, dissolved clay, cement, sulfate, phosphate, corrosion products (Fe, Ni, Cr), etc.) on waste degradation rate.

Because the PA model does not explicitly simulate chemical reactions, $\Upsilon = \Upsilon_{pH} \cdot \Upsilon_{SA} \cdot \Upsilon_\alpha \cdot \Upsilon_{Si} \cdot \Upsilon_{CCL}$ is a time-independent factor that can be adjusted in sensitivity or uncertainty propagation analyses. By contrast, the temperature dependence of the waste degradation rate (last term in Equation 2) is updated dynamically, as temperature is one of the solution variables of the coupled thermal-hydrological PA model.

Waste form degradation is often described by a fractional degradation rate, ω (s^{-1}), which is the rate with which the remaining waste mass degrades per year. The fractional waste degradation rate can be obtained from degradation experiments as the slope given by Equation 6

$$\omega = -\frac{\ln\left(m(t)/m(t + \Delta t\right)}{\Delta t} \tag{6}$$

where $m(t)$ is the mass of the waste form at a given time t. The fractional degradation rate ω can be considered temperature dependent based on the Arrhenius equation (Equation 2). The rate with which the mass of radionuclides in the waste form is reduced due to decay and congruent release is then given by Equation 7:

$$\frac{dm}{dt} = m(t) \cdot (\lambda + \omega) \tag{7}$$

The radionuclide mass encapsulated in the degrading waste matrix at time t is given by Equation 8:

$$m(t) = m_0 \cdot (1 - IRF) \cdot e^{-\lambda t} \cdot e^{-\omega (t - t_b)} \tag{8}$$

where m_0 (kg) is the initial inventory at time zero, and IRF is the instant release fraction, which is the fraction of certain semi-volatile radionuclides (specifically ^{129}I, ^{14}C, and Cs isotopes) that are rapidly released, mainly from spent nuclear fuel with high in-reactor irradiation (Johnson et al., 2023). The time-dependent rate q_{RN} (kg s^{-1}), with which the radionuclide mass remaining in the solid waste matrix is released to the pore fluid due to waste form degradation, is given by Equation 9:

$$q_{RN}(t) = m(t) \cdot \omega \tag{9}$$

While the fractional waste degradation model is typically used to describe the degradation of spent fuel assemblies, other waste forms such as vitrified, metallic, or ceramic waste forms placed into a disposal canister have an approximately cylindrical shape. The initial volume of a waste cylinder of radius R (m) and length L (m) is given by Equation 10:

$$V = \pi R^2 L \tag{10}$$

The volume of unreacted waste changes as its radius and length are reduced by degradation, as given by Equation 11:

$$dV = 2\pi R L\, dR + \pi R^2\, dL \tag{11}$$

The reduction in the radius (Equation 12) and the length (Equation 13) of the unreacted waste due to degradation is given by:

$$dR = \frac{q}{\rho_{WF}}\, dt \tag{12}$$

$$dL = 2\frac{q}{\rho_{WF}}\, dt \tag{13}$$

where q (kg m^{-2} s^{-1}) is the adjusted waste degradation rate of Equation 2, and ρ_{WF} (kg m^{-3}) is the density of the waste form. The volumetric waste degradation rate is therefore calculated as:

$$q_{WF}(t) = \frac{dV(t)}{dt} = 2\pi \frac{q}{\rho_{WF}} \left(L(t) \cdot R(t) + R(t)^2\right) \tag{14}$$

If the surface rate q is constant with time, the mass degradation rate of the waste form is given by:

$$q_{WF}(t) = 2\pi q \left(3\left(\frac{q}{\rho_{WF}}(t - t_b)\right)^2 - (L + 4R)\frac{q}{\rho_{WF}}(t - t_b) + R(L + R)\right) \tag{15}$$

If $L \gg R$, degradation from the two circular end faces of the cylinder can be ignored, and Equation 15 simplifies to Equation 16

$$q_{WF}(t) = 2\pi L r \left(R - \frac{q}{\rho_{WF}} \cdot (t - t_b)\right) \tag{16}$$

If q is time-dependent (e.g., due to the time-varying waste temperature), Equation 14 is evaluated numerically for each

waste element, with the cylinder's radius and length updated after each time step.

The waste form mass remaining in the canister is calculated by Equation 17:

$$m_{WF}(t) = m_{WF,0} - \int_{t_f}^{t} q_{WF}(\tau)d\tau \tag{17}$$

where $m_{WF,0}$ (kg) is the initial mass of the waste form. The radionuclide mass fraction in the waste form is given by Equation 18:

$$X_{WF}^{RN}(t) = m_{\mathrm{RN},0} \cdot (1 - IRF) \cdot e^{-\lambda t} \Big/ m_{WF,0} \tag{18}$$

Finally, the congruent radionuclide release rate from the waste form is given by Equation 19:

$$q_{RN}(\mathrm{t}) = q_{WF}(t) \cdot X_{WF}^{RN}(t) \tag{19}$$

For constant q and a cylinder that is relatively long, i.e., $L \geq 2R$, the waste form is fully degraded at time $t\,(q_{WF} = 0) = R{\cdot}\rho_{WF}/q$. For a more disk-shaped waste form, i.e., $L < 2R$, the waste form is fully degraded at time $t\,(q_{WF} = 0) = L/2{\cdot}\rho_{WF}/q$.

The instant release fraction (IRF) is implemented by specifying an initial radionuclide mass fraction dissolved in the water within the canister that yields the IRF's mass of the inventory, $m_{IRF} = m_0 \cdot IRF$. Furthermore, the initial inventory is reduced to $m_e = m_0 \cdot (1 - IRF)$ to properly reflect the fact that a smaller mass of radionuclides is encapsulated in the solid waste form. The mass m_{IRF} will be mobilized instantaneously at the time of canister failure, t_b, while mass m_e will be mobilized by congruent release as the waste forms dissolves.

The waste degradation and radionuclide release models described above are implemented in the iTOUGH2 simulation-optimization software (Finsterle et al., 2017; Finsterle, 2025), allowing for a fully integrated analysis of the impact of waste-form related parameters on overall performance of the repository system, as demonstrated in Section 3.

2.2 Post-closure performance assessment model

To examine the importance of source-term model parameters on the safety of a radioactive waste repository, a PA model is developed that combines the source-term model with key components of the engineered and natural barrier systems and integrates them into a coupled thermo-hydrological numerical model that simulates fluid flow, heat transfer, and radionuclide transport from the canisters to the accessible environment. The activity of the main safety-relevant radionuclides in drinking water extracted from a near-surface aquifer is calculated and multiplied by the nuclide's respective dose conversion factor (IAEA, 2003). Finally, the dose contributions from all tracked radionuclides are summed, and the maximum value over the entire performance period is determined and reported as the peak exposure dose, which is considered one of the main performance metrics of interest that represents long-term repository safety (e.g., Nagra, 2024). This general PA modeling approach is applicable to different repository types; in what follows, we use as an example the disposal of vitrified waste in a deep vertical borehole repository constructed in fractured, crystalline basement rock.

We use a simplified version of the model described in Finsterle et al. (2021b), which was developed to simulate the transport of radionuclides released from a deep vertical borehole repository. An array of parallel boreholes with a constant spacing of 50 m is modeled by taking advantage of vertical symmetry planes intersecting the borehole axis and the mid-plane between two neighboring boreholes. A total of 300 canisters are placed into a 1,500 m long disposal section, one canister every 5 m. Each canister holds three CSD-V[1] containers, each with a cylinder of vitrified waste with a length of 1.4 m and a radius of 0.2 m, from which heat and radionuclides are released according to the source-term model described in Section 2.1.

A schematic of the considered repository system is shown in Figure 1. The repository is assumed to be constructed in crystalline bedrock, which may be encountered at relatively shallow depths, immediately below a 500 m thick sedimentary cover, which also

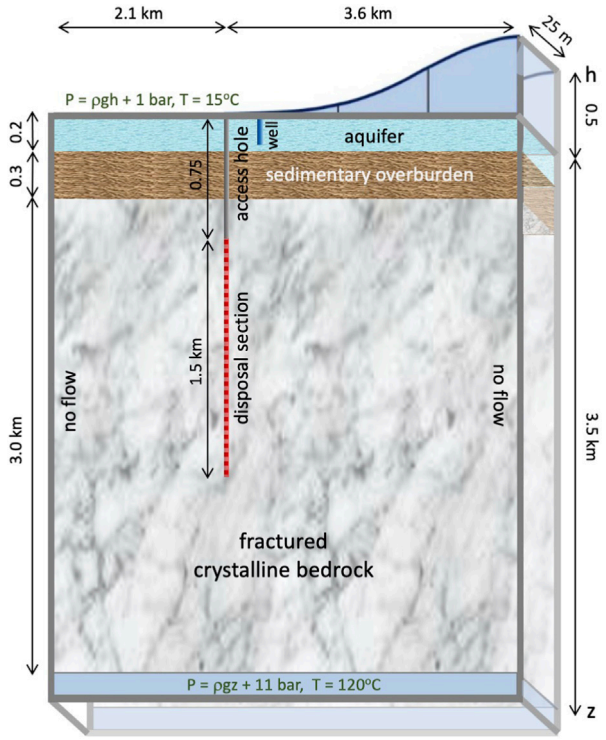

FIGURE 1
Schematic of model domain, representing symmetry cell of vertical borehole repository (not to scale). Radionuclides are released from the disposal section, indicated by the red dashed line; exposure dose is recorded at the location of the drinking water well, indicated by the blue line in the near-surface aquifer.

1 CSD-V stands for "Colis Standard de Déchets–Vitrifiés" ("Standard Waste Package–Vitrified"), which is a container designed for interim storage at the facility in La Hague, France. The analysis presented here is not specific to the waste generated at that facility

includes a 200 m thick drinking water aquifer. The disposal section extends between a depth of 750 and 2,250 m. A well 200 m from the access hole of the repository extracts drinking water from the aquifer. Regional groundwater flow is driven by topographic elevation changes, here represented by two 500 m high, parallel mountain ridges that act as recharge zones. Groundwater flows preferentially laterally from the mountain ridges towards the discharge zone near a river that runs along the center of the valley. The flow field is affected by the drinking water well, which is assumed to pump at a constant rate of 1,000 m^3 per year. Such a relatively small pumping rate leads to reduced dilution of the contaminated water and therefore a higher exposure dose. The narrow width of the symmetry cell ensures that essentially all radionuclides seeping into the aquifer will be captured by the well. In addition, a conservative, vertical upflow is introduced by specifying a constant pressure at the bottom of the model that is higher than the hydrostatic pressure. The hydrostatic pressure is affected by depth-dependent density changes due to the increase in pressure, salinity, and temperature, which is controlled by the mean annual surface temperature of 15 °C and an average geothermal gradient of 30 °C per kilometer.

At the depth of the repository, the granitic host rock is typically fractured, potentially providing pathways for advective radionuclide transport, which is retarded by diffusion into the essentially stagnant pore water of the rock mass between the connected fracture network. The degree of fracturing is related to the stress regime and is thus depth dependent. The discreteness of fractures, their connectivity, variability in aperture distribution, and gradient-dependent channeling effects lead to effective permeabilities that are heterogeneous and anisotropic. The key safety-relevant features of a crystalline geosphere—i.e., potentially fast fluid flow through a connected fracture network and radionuclide retention by matrix diffusion—are included in the model by a dual-continuum approach, with a depth-dependent trend of average fracture-network permeability (Achtziger-Zupančič et al., 2017) that is superimposed by geostatistically generated, spatially correlated and anisotropic variability. The exchange of fluids and radionuclides between the fracture and the matrix continua is controlled by the geometry of the fracture network, which is assumed to consist of two sets of planar, parallel, infinite fractures with an arbitrary angle between the two sets and a constant fracture spacing. The matrix is considered homogeneous. Global matrix-to-matrix fluid flow and radionuclide transport is allowed only in the vertical direction, consistent with the fact that the regional stress field at the depth of the repository likely generated subvertical fracture zones. For the current long-term analyses, some components of the engineered barrier system (i.e., the annulus between the canister and casing, the casing, and the cement between the casing and the borehole wall) are not individually discretized but represented by appropriate effective parameters that account for anisotropy in permeability between the axial and radial directions.

To summarize: The EBS is represented by an effective porous material with a strong axial-to-radial anisotropy; in the geosphere, fluid flow, heat transfer, and radionuclide transport through the fracture network is three-dimensional, with local exchange to the matrix continuum and global matrix-to-matrix flow and transport in the vertical direction.

The model domain is first discretized into a three-dimensional, structured Cartesian mesh with $69 \times 8 \times 104 = 57,408$ grid blocks in X, Y, and Z direction, respectively. The smallest grid blocks have dimensions of $dx = dy = 0.31$ m, yielding the desired canister cross section of $\pi \cdot r_c^2 = 0.096$ m^2. Element sizes in X direction gradually increase and remain constant at 10 m up to a distance of 200 m from the borehole, after which they gradually increase again to a maximum dx of 500 m at the outer lateral boundaries of the model. In Y direction, the same increase in grid-block sizes away from the borehole is used up to the symmetry plane at $y = 25$ m. In vertical direction, grid spacing is constant at $dz = 25$ m from the land surface to a depth of 2,350 m (i.e., 100 m below the bottom of the borehole) after which layer thicknesses gradually increase to a maximum of 135 m at the bottom of the model. In a second mesh generation step, each grid block representing the crystalline bedrock is divided into two overlapping elements representing the fracture and matrix continuum, which are locally connected to each other, as described above. This results in a finite volume mesh with a total of 108,890 grid blocks and 216,724 connections between them. Five equations are solved for each grid block—one for pressure, temperature, salinity, and the mass fractions of ^{129}I and ^{135}Cs—for a total degree of freedom of 544,450. More details about processes, material properties, discretization in space and time, and the solution algorithm can be found in Muller et al. (2019) and Finsterle et al. (2020), Finsterle et al. (2021a), and Finsterle et al. (2021b).

The key processes considered in this study are non-isothermal flow of water and brine. Decaying radionuclides are transported by advection and diffusion, and they may be retarded by reversible sorption onto the solid phase. Heat is transported by conduction and convection. Porosity changes linearly as a function of pore pressure and temperature using volumetric pore compressibility and thermal expansivity. Details about the physical processes and the corresponding mathematical model and numerical scheme can be found in the documentation of the TOUGH2 code (Pruess et al., 2012), which is implemented in the iTOUGH2 simulation-optimization framework (Finsterle et al., 2017). iTOUGH2 is used in this study to take advantage of enhanced user features (Finsterle, 2025), specifically the capability to seamlessly integrate steady-state initialization runs with the transient simulation after repository construction and waste emplacement, which requires changes in properties and boundary conditions at discrete times. Moreover, the fractional and cylindrical waste degradation models and corresponding radionuclide releases described in Section 2.1 are implemented in iTOUGH2, where the factors influencing the source term are adjustable parameters for the calculation of composite sensitivity measures (Finsterle, 2015) as well as for inverse modeling, global sensitivity and uncertainty propagation analyses. In the current study, iTOUGH2 will be used for local sensitivity analyses and Monte Carlo simulations for examining prediction uncertainties, using Latin hypercube sampling to make sure parameter realizations cover the entire range and are in conformance with the assumed occurrence probabilities (Zhang and Pinder, 2003).

Properties of the main engineered and natural materials are listed in Table 1; they are not site specific but are considered representative of a generic borehole repository in a fractured, crystalline host rock. Note that this study focuses on the *relative*

10.3389/fnuen.2025.1729916

TABLE 1 Relevant material properties.

Parameter	Units	Value
Waste		
Porosity	$m^3\ m^{-3}$	0.1
K_d value (congruent release, no sorption)	m^3 kg	0.0
Canister		
Absolute permeability, canister intact	m^2	0.0
Absolute permeability, canister corroded	m^2	10^{-16}
Effective EBS (annulus, casing, cement), plug and backfill		
Absolute permeability, axial	m^2	10^{-16}
Absolute permeability, radial, casing intact	m^2	0.0
Absolute permeability, radial, casing corroded	m^2	10^{-18}
Absolute permeability, plug	m^2	10^{-18}
Absolute permeability, backfill	m^2	10^{-16}
Crystalline Host Rock		
Absolute permeability, fracture network		
Horizontal reference permeability at depth of 500 m	m^2	10^{-17}
Vertical reference permeability at depth of 500 m	m^2	10^{-16}
Permeability reduction factor with depth	log () km^{-1}	−1.0
Geostatistical permeability modifier (heterogeneity)		
Spherical semivariogram		
Sill value	log ()	1.0
Correlation length, horizontal	m	100.0
Correlation length, vertical	m	1000.0
Fracture spacing (affects retardation by matrix diffusion)	m	100.0
Absolute permeability, matrix	m^2	10^{-20}
Utilization factor (affects retardation by matrix diffusion)	-	0.01
Porosity, fracture network (affects advective transport)	$m^3\ m^{-1}$	0.01
Porosity, matrix (affects retardation by matrix diffusion)	$m^3\ m^{-3}$	0.01
Rock grain density (affects sorption and thermal diffusivity)	kg m^{-3}	2700.0
Overburden		
Absolute permeability, horizontal	m^2	10^{-14}
Absolute permeability, vertical	m^2	10^{-15}
Porosity	$m^3\ m^{-3}$	0.15
Aquifer		
Absolute permeability, horizontal	m^2	10^{-13}
Absolute permeability, vertical	m^2	10^{-14}
Porosity	$m^3\ m^{-3}$	0.25

impact of changes in source-term parameters on peak exposure dose calculated for a generic reference case; the purpose is not to justify the *absolute* peak dose value, which depends on site-specific properties and conditions. While each material is associated with a full set of thermal and hydrological parameters, only a small subset of these parameters is provided, selected based on their significance for the storage and flow of fluids and heat as well as radionuclide transport within the respective material.

Only two radionuclides, ^{129}I and ^{135}Cs, are tracked in the PA model, down-selected from a comprehensive list of radionuclides present in the waste form according to their relative safety-relevance, which is estimated in a two-step approach based on the

radionuclide's inventory, half-life, specific activity, and dose coefficient, as well as their retardation in the geosphere, which is related to sorption and matrix diffusion. Table 2 lists key radiological and transport properties of the two safety-relevant radionuclides.

2.3 Degradation parameters for vitrified waste

In the example discussed below, we consider the vitrification of high-level radioactive waste in a lanthanide borosilicate (LaBS) glass matrix. LaBS glasses are primarily composed of lanthanide oxides, silica, alumina, and boron oxide, as well as minor components such as barium, lead, or strontium oxide (Jantzen, 2011). Compared to traditional alkali aluminoborosilicate glasses, LaBS glasses are chemically more durable and exhibit higher glass transition temperatures, melting temperatures, and radionuclide solubilities (Jantzen, 2011). Compared to traditional alkali aluminoborosilicate glasses, LaBS glasses are chemically more durable and exhibit higher glass transition temperatures, melting temperatures, and radionuclide solubilities (Peeler et al., 1999). Other favorable qualities of these glasses include the presence of significant quantities of neutron absorbers (lanthanide oxides) that permit increased loading of fissile materials into the glass with negligible increases in the risk of criticality. Due to these characteristics, LaBS glasses have been explored as an effective waste form for the encapsulation of high-level radioactive wastes generated by existing and future facilities for the reprocessing and recycling of spent nuclear fuel.

Several properties affect the actual alteration rate of LaBS glass waste forms in a deep geological repository. These include (a) intrinsic waste form parameters such as rate constant and activation energy, (b) physical parameters such as surface area, (c) environmental factors such as temperature, leachate composition, and the precipitation of secondary phases, and (d) other factors such as radiation/radiolysis effects. The degradation parameters of LaBS glass along with some repository conditions that affect glass alteration are summarized in Table 3. The reference set is generic; some of the values are chosen to better demonstrate their potential impact on radionuclide release and repository performance during the sensitivity analyses, which are performed for a subset of the parameters by perturbing the parameter value one at a time within the range indicated in Column 3 of Table 3. A parameter scaling factor σ_p is given in Column 4, which represents the approximate variation or uncertainty of the parameter. The same value is used as the parameter uncertainty to be propagated through the PA model to estimate the prediction uncertainty of the peak exposure dose and the time it occurs (see Section 3.3 below). Both the reference values of the waste degradation parameters and their expected uncertainty will likely be adjusted once waste-form- and site-specific characterization data become available.

3 Simulation results

Having established the governing equations and parameter dependencies, we further evaluate how variations in the source-term model translate into long-term repository performance metrics. These results provide quantitative insights into which uncertainties may most strongly influence safety predictions.

3.1 Reference case

We first present the prediction results obtained with the reference parameter set listed in Column 2 of Table 3. While the PA model calculates a comprehensive set of primary solution variables and derived quantities at each location within the model domain, we focus here on a small subset that highlights the system response to changes in the radionuclide source term and the exposure dose at the land surface, which is the performance metric of overall repository safety.

Figure 2A shows the total release rate of ^{129}I and ^{135}Cs from all canisters. The mass release rate, which depends on the parameters of

TABLE 2 Radiological and transport properties of safety-relevant radionuclides.

Radionuclides		
^{129}I		
Half-life	yr	1.57×10^{7}
Specific activity	Bq kg^{-1}	6.53×10^{9}
Ingestion dose coefficient (IAEA, 2003)	Sv Bq^{-1}	1.10×10^{-7}
Inventory (Caruso et al., 2017)	kg canister^{-1}	2.90×10^{-2}
Instant release fraction	kg kg^{-1}	0.0
K_d value (Nagra, 1994)	m^3 kg^{-1}	3.00×10^{-5}
Diffusion coefficient in bulk water	m^2 s^{-1}	2.00×10^{-9}
^{135}Cs		
Half-life	yr	2.30×10^{6}
Specific activity	Bq kg^{-1}	4.26×10^{10}
Ingestion dose coefficient (IAEA, 2003)	Sv Bq^{-1}	2.00×10^{-9}
Inventory (Caruso et al., 2017)	kg canister^{-1}	2.77×10^{0}
Instant release fraction	kg kg^{-1}	0.0
K_d value (Nagra, 1994)	m^3 kg^{-1}	5.00×10^{-2}
Diffusion coefficient in bulk water	m^2 s^{-1}	2.00×10^{-9}

TABLE 3 Reference value of waste-degradation- and radionuclide-release-related parameters for LaBS glass.

Parameter	Value	Range	σ_p	References/Comment
Waste loading factor	1.0	[0.5, 1.5]	0.1	Includes changes in waste loading and canister spacing
Degradation rate on exposed waste surface, log (q_0 [kg m^{-2} s^{-1}])	−11	[-12, −10]	1.0	Ramsey et al. (1995); Peeler et al. (1999), Marra and Ebert (2003); Marra (2006), Crawford et al. (2007); Curti (2022)
pH	8	[7, 9]	0.5	Marra and Ebert (2003); Ebert (2006)
pH power law exponent, μ	0.4	[0.2, 0.6]	0.1	Marra and Ebert (2003), Ebert (2006); Vienna et al. (2018)
Activation energy, E_a (kJ mol^{-1})	40	[20, 60]	10	Marra and Ebert (2003); Ebert (2006); McLachlan et al. (2024)
Surface area increase, Υ_{SA}	15	[5, 40]	5	Peters and Slate (1982); Kessler (2002); Jones (2006); Nagra (2014b); Curti (2022)
Radiation and chemical effects $\Upsilon_\alpha \cdot \Upsilon_{CCL}$	2	[1, 5]	1	Mougnaud et al. (2016), Mougnaud et al. (2018), De Echave (2018); Tribet et al. (2021)
Residual rate factor, log (Υ_r)	−2	[-4, 0]	1	Curti (2022); McLachlan et al. (2024)
Instant release fraction, *IRF* (%)	0	[0, 100]	n/a	Includes instant waste mobilization case
Duration of affinity effects log ($(t_e - t_b)$ [yr])	4	[3, 5]	0.5	Fournier et al. (2014); McLachlan et al. (2024)
Canister breach time, log (t_b [yr])	4	[3, 5]	1	King et al. (2024); includes early canister failure scenario

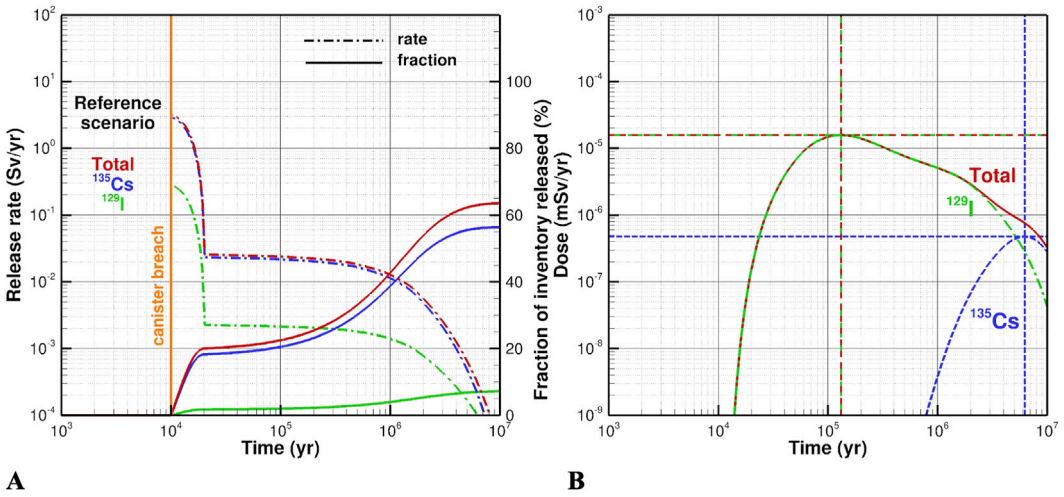

FIGURE 2
(A) Rate and cumulative dose released from waste canisters (dash-dotted lines: release rate; solid lines: fraction of inventory), and **(B)** exposure dose (dash-dotted lines: ^{129}I; dashed lines: ^{135}Cs; solid lines: sum of ^{129}I and ^{135}Cs dose curves). as a function of time for the reference scenario.

Table 3 controlling waste degradation and congruent radionuclide mobilization according to the source-term model described in Section 2.1, is converted to Sieverts per year (Sv/yr) to allow for a direct comparison of the release rate at the underground disposal section of the repository with the eventual exposure dose at the land surface. The difference between the two rates reveals the effectiveness of the natural barrier system. Figure 2A also shows the fraction of the inventory released to the near field; the initial inventory of ^{129}I and ^{135}Cs in all 300 canisters amounts to a total dose of approximately 80,000 Sv.

Radionuclide release starts at the time the canisters are breached. The initial release rate is highest because (a) the exposed surface area of the waste form is at its maximum, (b) the surface-specific degradation rate q is not yet reduced by affinity effects, (c) reservoir temperature may still be elevated from decay heat release, and (d) no significant radioactive decay, which lowers the activity of ^{129}I and ^{135}Cs in the system, has occurred within the canister. During the first 10,000 years after canister breach, the waste degradation rate is reduced as the orthosilicic acid activity approaches chemical equilibrium, at which point the rate has been lowered by a factor of $\Upsilon_r = 0.01$. Waste degradation and radionuclide release proceed at lower and continuously decreasing rates, as the surface area of the waste-form cylinder shrinks, temperatures approach ambient values, and radionuclides in the canister decay. For the reference parameter set, the waste form is never completely dissolved even after 10 million years, at which point a waste-form cylinder of length 1.14 m and radius 0.07 m remains at the locations of each of the inner CSD-V containers,

highlighting the effectiveness of the LaBS waste form to retain radionuclides for very long times. As a result of containment and slow release, only about 60% of the inventory's initial activity is released from the canisters. Finally, it is noted that ^{135}Cs has a higher contribution to the release rate than ^{129}I, initially by a factor of 11.3, which is the ratio of their respective inventories, specific activities, and dose coefficients (see Table 2). The dominance of ^{135}Cs release declines with time due to its shorter half-life.

^{135}Cs—as well as other radionuclides initially present in the waste form—may indeed have significantly higher radiological consequences than ^{129}I if it were released from a breached canister at the land surface, or if contaminated groundwater were extracted directly from the near field of the repository. However, it is important to recall that the safety of the repository is controlled by the performance of the natural barrier system with its various retention mechanisms that considerably delay exposure, thus reducing risks and changing the order of the radionuclides' relative safety relevance. Many of the radionuclides in the inventory have an insignificant contribution to peak dose due to the effectiveness of the natural barrier system, while others (such as ^{129}I) that seem less problematic at the source become the most safety relevant. The screening process used to estimate each radionuclide's relative safety-relevance is based on key metrics that account for characteristics of the radionuclide itself as well as its migration from the canister to the dose recipient. While it is essential to have a source-term model that accurately calculates the release of radionuclides into the geosphere, it must be integrated into a suitable PA model that simulates flow and transport processes and provides estimates of the ultimate exposure dose, which reflects repository safety.

Figure 2B shows the contributions of ^{129}I and ^{135}Cs to the annual exposure dose from the ingestion of drinking water extracted from the aquifer above the repository. The non-sorbing ^{129}I is highly mobile despite being somewhat retarded by matrix diffusion. It reaches its peak dose of 1.6×10^{-5} mSv yr^{-1} after about 130,000 years, a time too short for radioactive decay to reduce its concentration. Because the source term is not a single pulse, but radionuclides are released over an extended time with a declining rate, the breakthrough curve is relatively flat and exhibits a long tail.

By contrast, ^{135}Cs arrives at the land surface very late (after approximately 6 million years) as its migration is retarded by comparatively strong adsorption to the fracture surfaces and the grains of the rock matrix. Despite its long half-life of 2.3 million years, this prolonged travel time is sufficient for radioactive decay to reduce the ^{135}Cs mass by about a factor of six. The combination of radioactive decay and the lowering of the concentration peak due to adsorption leads to a considerable amplitude reduction of the ^{135}Cs breakthrough curve. As a result of different magnitudes and temporal separation of the ^{129}I and ^{135}Cs breakthrough curves, the peak dose of the sum of the two radionuclides is completely dominated by, and thus essentially identical to, that of ^{129}I. Note that the peak dose of 1.6×10^{-5} mSv yr^{-1} is almost four orders of magnitude below a typical dose standard of 0.1 mSv yr^{-1}.

The reference results shown in Figure 2 depend on numerous conceptual assumptions and simplifications, as well as on uncertainties in the model's many input parameters. For the purpose of the current analysis, we focus on parameters of the source-term model and examine their impact on predictions of peak exposure dose through standard sensitivity analyses (Section 3.2) and a sampling-based uncertainty propagation analysis (Section 3.3).

3.2 Sensitivity analysis

The purpose of the sensitivity analyses is (a) to get physical insights into how the various processes implemented in the source-term model affect radionuclide release from the canisters, and (b) to identify the relative influence of source-term model parameters on the prediction of exposure dose, which helps formulate criteria for how accurately waste-form-related parameters need to be determined as not to induce unacceptably high prediction uncertainties that would render PA calculations less conclusive. Each sensitivity analysis presented below consists of perturbing one parameter at a time from its reference value and then calculating and visualizing the system response. The local parameter range covered by the perturbations is indicated in Table 3. Note that changing the waste loading factor leads to a proportional change in the release rates and peak dose. The impact of pH is also a simple proportionality factor as given by Equation 3. Similarly, the parameters modifying the degradation rates by a constant factor exhibit the same sensitivity behavior as changes in the intrinsic rate, scaled by the σ_p ratio. Therefore, discrete sensitivity analyses are discussed for only six of the 11 parameters listed in Table 3. All 11 parameters will be varied during the uncertainty propagation analysis discussed in Section 3.3.

Figure 3 shows the influence of changes in the canister breach time on the sum of the ^{129}I and ^{135}Cs release rates and the cumulative release fraction of the inventory as well as on the individual and combined exposure doses. Changing the time of canister breach leads to a corresponding shift in the time when peak dose occurs. However, the peak dose itself remains essentially unchanged. Even if a very durable canister with a lifetime of 100,000 years is used, the peak dose is reduced only by the amount of radioactive decay occurring during the time shift, i.e., the period when the radionuclides were still contained in the canister, with some minor secondary effects related to changes in the temperature. Canister durability may be an important design criterion to prevent the early release of highly active radionuclides. However, highly active isotopes are typically short-lived, which means that they have decayed to insignificant levels once they arrive at the land surface, at least for the nominal case. Moreover, even in the very unlikely event that all canisters are breached immediately after repository closure, the radionuclides are still encapsulated in the waste form, which degrades very slowly even under the elevated temperatures prevalent during the first few decades of the thermal period. Temperatures encountered by the waste form range from 38 °C for shallow canisters after the thermal period, and 172 °C for the deepest canisters at the peak of the thermal period. Finally, the risks and consequences of severe failure of both the canister and waste form are partly addressed by pre-closure canister and waste-form performance requirements.

The criterion of a very long canister lifetime—with the considerable costs associated with the fabrication of such canisters—is sometimes driven by the attempt to demonstrate that the engineered barrier system by itself meets the long-term

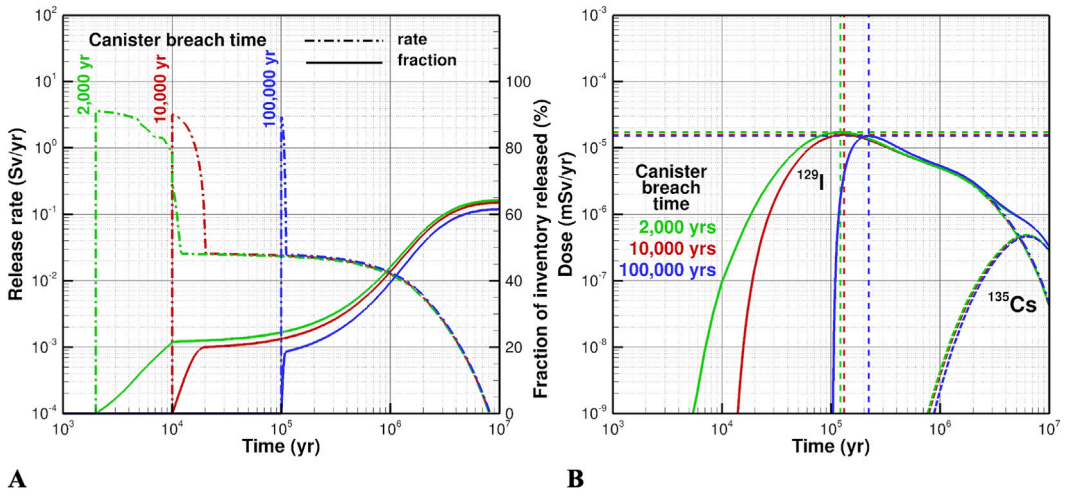

FIGURE 3
Sensitivity of **(A)** rate and cumulative dose released from waste canisters (dash-dotted lines: release rate; solid lines: fraction of inventory), and **(B)** exposure dose (dash-dotted lines: ^{129}I; dashed lines: ^{135}Cs; solid lines: sum of ^{129}I and ^{135}Cs dose curves) with respect to canister breach time.

dose standard in the case of disruptive events that render the natural barrier system ineffective. Occurrence probabilities and consequences of such disruptive scenarios can be mitigated by proper site selection. Moreover, PA calculations for deep borehole repositories show considerable robustness and resilience to such adverse conditions and events (Finsterle et al., 2020; Finsterle et al., 2021a; Finsterle et al., 2021b).

Figure 4 reveals the sensitivities with respect to the intrinsic waste degradation rate q_0, a parameter that can be inferred from leaching experiments, but may have relatively large estimation uncertainties due to its low value for materials (such as LaBS glasses) used as the matrix for the encapsulation of radioactive isotopes. Increasing or decreasing q_0 by one order of magnitude leads to a corresponding change in the initial radionuclide release rates immediately after canister breach. For the highest rate, about 85% of the radionuclides are released within the first 10,000 years after canister breach. However, for such a high intrinsic rate q_0, the mass degradation rate of the waste form (q_{FW}; see Equation 14) declines more quickly as the surface area of the cylindrical waste form shrinks faster compared to the reference case. Nevertheless, the entire waste form is consumed after about 1 million years. This rate profile can be described as a pulse release of most of the inventory, while for the two cases with a lower intrinsic rate, radionuclides are continually released over the entire performance period, as reflected by the long-tailed breakthrough curves shown in Figure 4B. The ratios of the peak exposure doses for the two low-rate cases are approximately proportional to the ratio of the intrinsic waste degradation rate. However, the dose ratio between the reference

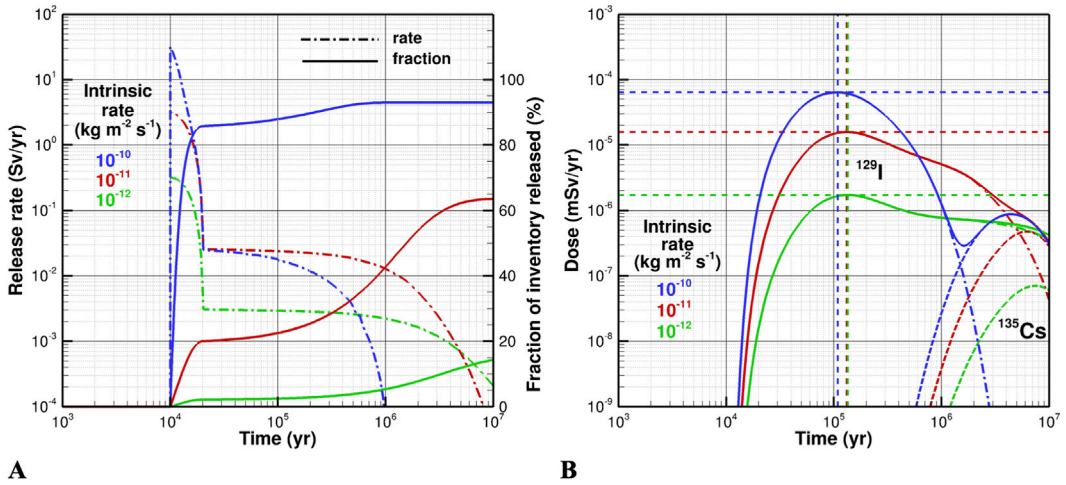

FIGURE 4
Sensitivity of **(A)** rate and cumulative dose released from waste canisters (dash-dotted lines: release rate; solid lines: fraction of inventory), and **(B)** exposure dose (dash-dotted lines: ^{129}I; dashed lines: ^{135}Cs; solid lines: sum of ^{129}I and ^{135}Cs dose curves) with respect to intrinsic waste degradation rate.

case and the high-rate case is less than a factor of ten because of the secondary effect of a faster reduction in the waste form's surface area, as described above. Nevertheless, it is apparent that the intrinsic rate is one of the main parameters affecting peak dose.

The same impact is expected from the factors that directly increase the degradation rate by a constant, such as the factors accounting for the impact of waste-form fracturing (Υ_{SA}), radiation (Υ_{α}), leachate composition (Υ_{CCL}), and pH effects (Υ_{pH}). The relative impact of these factors depends on their expected uncertainty, which is expressed by σ_p (see Table 3).

Figure 5 shows the influence of changing the maximum rate-reduction factor (or, equivalently, the residual rate q_r), which represents complex chemical affinity effects that lead to the formation of a passivating gel layer, moving the reaction front from the surface into the glass matrix, thus reducing the alteration rate as a function of time (see $\Upsilon_{Si}(t)$, Equations 3–5). In the reference case, it is assumed that the rate is reduced by a factor of 100 over a period of 10,000 years, which considerably slows waste degradation. If no affinity effects and thus no rate reduction occurs, i.e., if $\Upsilon_{Si} = 1$ (green curves), waste degradation remains high, and the entire waste form is consumed after about 200,000 years. This again results in an approximate pulse release of radionuclides, which leads to a higher peak dose compared to the case where affinity effects spread out the release of radionuclides over a very long time, which flattens the dose breakthrough curve. Interestingly, if the affinity effects are very strong and lead to a drastic reduction in the degradation rate (blue curves), the source term also has the characteristics of a pulse release, albeit only releasing about 20% of the inventory. Only in the intermediate case (the reference case, shown in red) is the reduced degradation rate still high enough to release about 40% of the inventory, creating the long-tailed dose breakthrough curve discussed previously. The peak dose, however, is controlled by the fast release of the initial 20% of the inventory, which is essentially the same amount for both the reference case (red) and the strong-affinity case (blue), leading to essentially the same peak dose.

It can be concluded that the presence or absence of affinity effects influences the peak dose. However, whether the rate reduction is on the order of a factor of 10 or much greater has no further influence on repository performance. This may also affect the conclusions about a possible rate resumption due to the precipitation of crystalline secondary phases (Thorpe et al., 2021). If that rate resumption is limited in magnitude or occurs after a prolonged period of waste degradation at the residual rate q_r, rate resumption is unlikely to lead to a dose that exceeds the primary peak value. Even if rate resumption reverts to the initial forward rate, the volume of waste being dissolved is smaller because of a reduced waste form surface area, and the amount of congruently released radionuclides is further reduced because of inventory decay. Finally—unlike the pulse release immediately after canister breach—rate resumption occurs gradually, leading to a flattening of the breakthrough curve at the land surface.

While Figure 5 shows the impact of the strength of affinity effects, Figure 6 examines the influence of how fast the degradation rate is reduced from the intrinsic rate q_0 to the residual rate $q_r = q_0 \cdot \Upsilon_{Si}(t_e)$. The duration of this rate-drop regime needed to transition from the forward to the residual rate regime (Thorpe et al., 2021) depends on many factors. If chemical equilibration progresses slowly, degradation rates are high for a longer period, leading to a higher peak dose. If chemical affinity processes are very fast, only a small fraction of the inventory is released at the initial high rate, while the rest is released with a low rate of q_r over a long period, leading to a comparatively flat breakthrough curve with a lower peak dose that occurs at a later time (see green curve in Figure 6B).

The temperature effect on degradation rates—as described by the Arrhenius equation—is examined next. We first note that in all results discussed so far, temperature effects are included, with each canister having its own waste degradation rate in accordance with the local temperature conditions, which is depth-dependent given the assumed geothermal gradient of 30 °C km^{-1}. For example, in the reference case, waste degradation in the deepest canister is

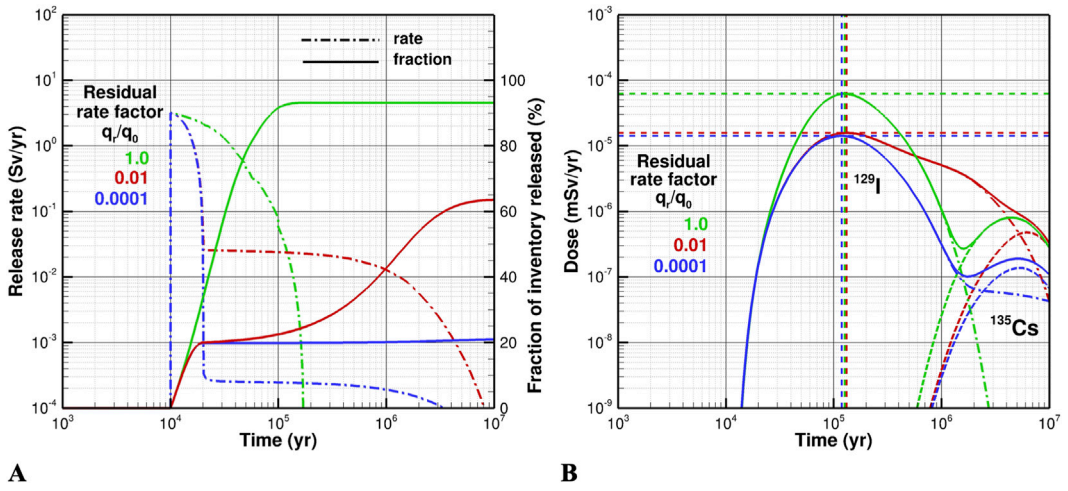

FIGURE 5
Sensitivity of **(A)** rate and cumulative dose released from waste canisters (dash-dotted lines: release rate; solid lines: fraction of inventory), and **(B)** exposure dose (dash-dotted lines: ^{129}I; dashed lines: ^{135}Cs; solid lines: sum of ^{129}I and ^{135}Cs dose curves) with respect to rate reduction due to affinity effects.

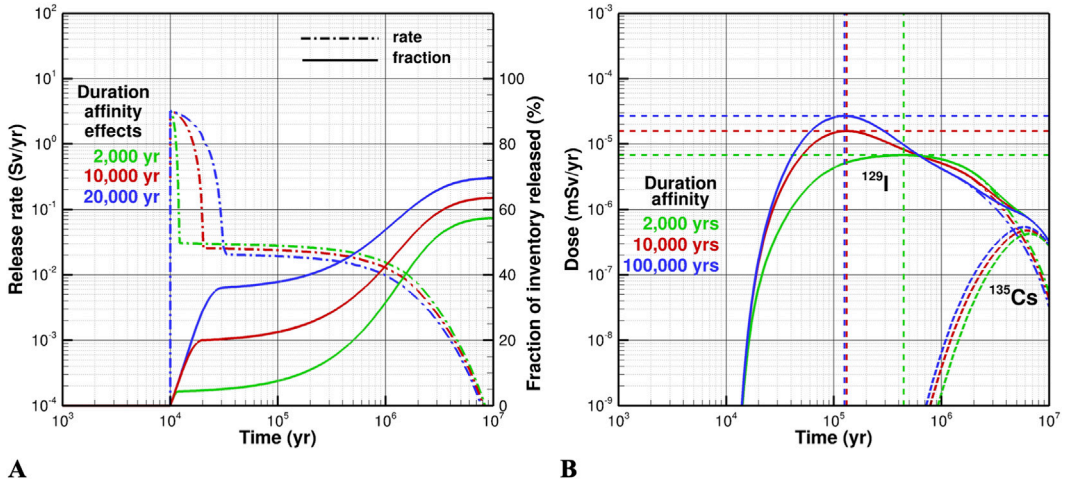

FIGURE 6
Sensitivity of **(A)** rate and cumulative dose released from waste canisters (dash-dotted lines: release rate; solid lines: fraction of inventory), and **(B)** exposure dose (dash-dotted lines: ^{129}I; dashed lines: ^{135}Cs; solid lines: sum of ^{129}I and ^{135}Cs dose curves) with respect to duration of affinity effects.

approximately seven times faster than in the shallowest canister due to an ambient temperature difference of 45 °C. The temperature increase caused by the waste's decay heat may further accelerate glass degradation. However, the generated decay heat declines relatively fast, with the maximum temperature reached after just a few years, and temperatures approaching their pre-disposal ambient conditions within a few hundred years. If the canister is not breached until after the early portion of the thermal period, the additional impact of repository-induced temperature changes on waste-form degradation is likely negligible.

Figure 7 shows the sensitivity of peak dose to changes in the activation energy, which is the adjustable parameter that controls the temperature dependence of waste degradation. In the examined scenario, the temperature of the repository at the time of canister breach (i.e., 10,000 years) is lower than the reference temperature of T_0 = 90° C. As expected, when $T(t) < T_0$, the lower the activation energy, the higher the waste degradation rate, with a corresponding sharpening of the initial release pulse and thus an increased peak dose. Note that if the canisters were breached during the early portion of the thermal period, where $T(t) > T_0$, lower values of activation energy would correspond to lower waste degradation rates, and the opposite trend would be observed until the temperature of the system falls below that of the reference temperature.

Finally, having established that peak dose is sensitive to the kurtosis and amplitude of the source term, we consider the instant release of a fraction of the inventory at the time of canister breach, including the bounding case in which all radionuclides are immediately mobilized. Instant release is only assumed for radionuclides (specifically ^{129}I) that have the

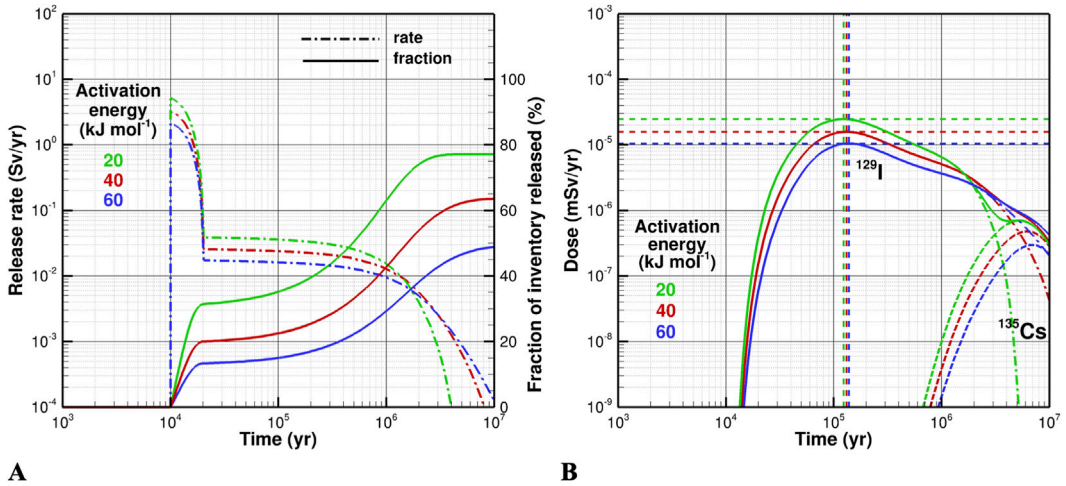

FIGURE 7
Sensitivity of **(A)** rate and cumulative dose released from waste canisters (dash-dotted lines: release rate; solid lines: fraction of inventory), and **(B)** exposure dose (dash-dotted lines: ^{129}I; dashed lines: ^{135}Cs; solid lines: sum of ^{129}I and ^{135}Cs dose curves) with respect to activation energy.

tendency to accumulate in gaps and on surfaces of pellets and cracks in spent nuclear fuel assemblies. However, no such accumulations are expected in vitrified waste. Nevertheless, we consider the unrealistic case with an *IRF* of 100%. While unrealistic, this scenario is considered useful as it provides an upper bound for the peak dose, which can also be interpreted as a case where repository performance relies almost exclusively on the natural barrier system, discounting long-term encapsulation of the radionuclides in the waste form, ignoring solubility limits, and assuming no adsorption occurs on corrosion products or other materials within the engineered barrier system. Note that none of the other parameters of the source-term model enter this extreme scenario, with the exception of the waste loading factor, which translates linearly into a corresponding change in the peak dose.

Figure 8A confirms that an *IRF* of 20% leads to the immediate release of that fraction of the inventory, verifying the correct implementation of the *IRF* feature in the PA model. Since the radionuclide mass encapsulated in the solid glass matrix is 20% less compared to the reference case, the release rates with a non-zero *IRF* are lower throughout the remainder of the waste form's degradation. Instant release of 20% of the inventory creates a sharper release pulse, which increases peak dose by about 50%—i.e., more than the *IRF* itself—but reduces the radionuclide mass in the tail of the breakthrough curve (see Figure 8B).

The bounding case with *IRF* = 100% leads to the highest peak dose of 6.6×10^{-5} mSv yr^{-1}. This dose is only about four times higher than the reference case. While unrealistic (if not physically impossible), this result is reassuring. It suggests that (a) in the absence of any information about waste-form degradation, and (b) making the most conservative assumption about radionuclide releases from the canister and its further retention in the engineered barrier system, the peak dose increases by less than an order of magnitude. This systematic shift is likely less than the uncertainties associated with the estimation of peak dose as part of such performance calculations.

3.3 Uncertainty propagation analysis

In the previous section, the source-term parameters were perturbed one at a time. These sensitivity analyses revealed considerable non-linearities in the dose response above a vertical borehole repository, with curves of radionuclide releases crossing each other and non-symmetric influences on peak dose. This calls for a sampling-based method to evaluate the impact of parameter uncertainties on the predicted performance metrics. Monte Carlo simulations with Latin hypercube sampling are used, drawing normally or log-normally distributed values around the reference parameter set with the standard deviation given in Column 4 of Table 3. The sample distribution is truncated at the bounds given in Column 3 of Table 3. It is further assumed that the uncertainties in the parameters are uncorrelated to each other. This is considered appropriate given that most of the source-term parameters are determined independently. An exception might be the experimentally determined intrinsic waste degradation rate, q_0, which could be affected by errors in pH, temperature, and other variables measured to characterize the test conditions. Similarly, the estimates of the activation energy E_a (Equation 2) or the pH exponent η (Eq. 2a) from leaching experiments may be weakly correlated to each other due to errors in the measured pH or temperature. However, the resulting correlations are expected to be minor and are unlikely to change the conclusions drawn from PA calculations. Finally, a small sample size of 500 realizations is simulated, which—in the context of this study—is considered sufficient to illustrate the degree of prediction uncertainty caused by assumptions about the radiological source-term model parameters. All other parameters,

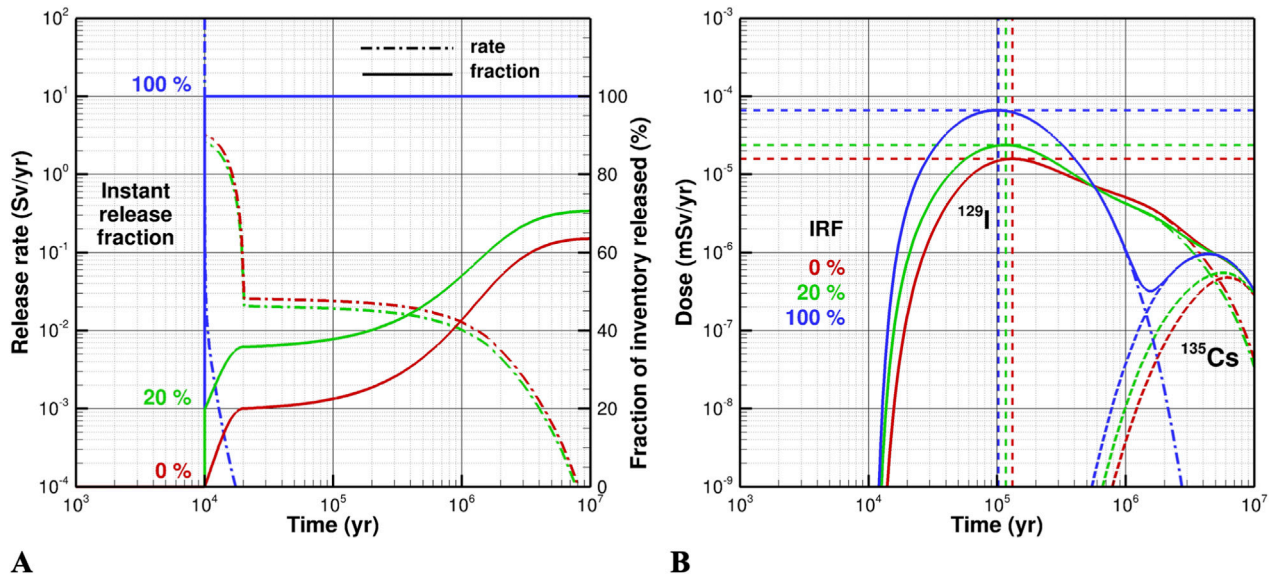

FIGURE 8
Sensitivity of **(A)** rate and cumulative dose released from waste canisters (dash-dotted lines: release rate; solid lines: fraction of inventory), and **(B)** exposure dose (dash-dotted lines: ^{129}I; dashed lines: ^{135}Cs; solid lines: sum of ^{129}I and ^{135}Cs dose curves) with respect to instant release fraction.

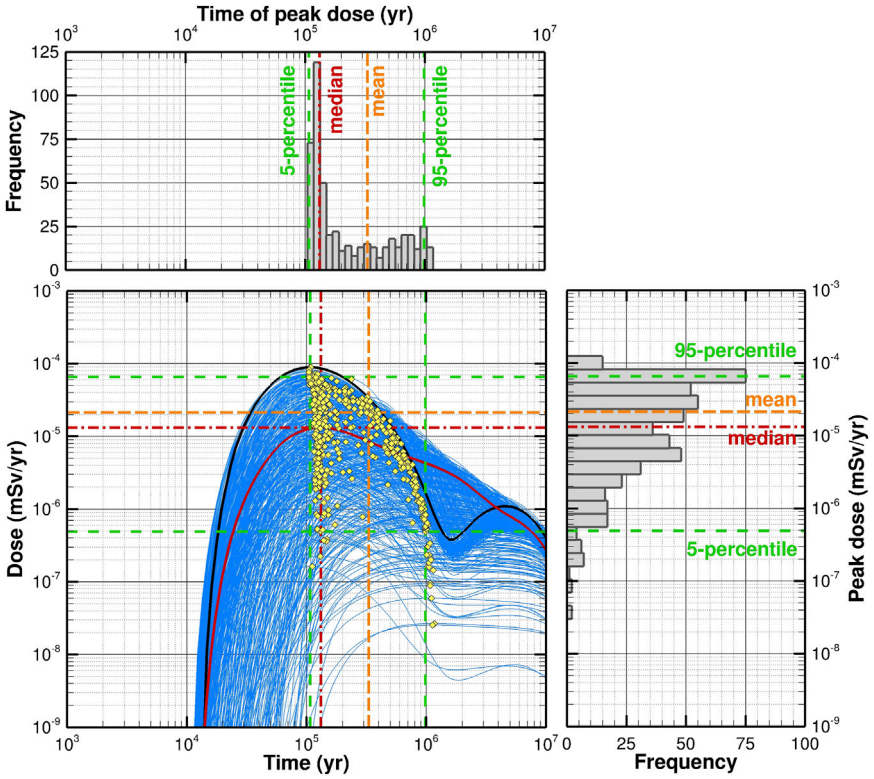

FIGURE 9
Illustration of prediction uncertainty caused by uncertainties and variabilities in radiological source-term parameters using Monte Carlo simulations. The yellow diamonds indicate the peak exposure dose for each of the 500 realizations. The thick black line is the realization leading to the highest peak dose; the thick red line is the result from the reference case, which also generates the median peak dose.

including thermal-hydrological properties and related flow and transport parameters, are fixed.

Figure 9 shows the dose breakthrough curves for the 500 random realizations along with the histograms of the peak dose and its time of occurrence. The reference case, which is close to the median peak dose, is highlighted in red; the realization leading to the highest peak dose value is shown in black. The 5th and 95th percentiles (green) are directly determined from the set of results ordered by their peak-dose and peak-dose-time values.

Figure 9 illustrates that various combinations of source-term parameters lead to a wide range of peak dose values; however, they are bounded by inherent, physical constraints. Only a few realizations exceed the peak dose value obtained by the *IRF* = 100% scenario (see Figure 8B), mainly because that bounding case was run with the reference waste loading factor of 1.0, whereas the radionuclide inventory is considered an uncertain parameter during the Monte Carlo simulations, with about half of the sampled realizations having waste loading factors greater than 1.0. If waste loading and canister spacing is known, the corresponding simulation with an *IRF* of 100% still provides a robust estimate of the upper bound for peak dose. The fact that many breakthrough curves cross each other, and that the histograms are non-symmetric and likely multimodal is a clear indication that the exposure dose is a strongly nonlinear function of the source-term input parameters.

The individual peak dose values obtained by each of the 500 Monte Carlo realizations (shown as yellow diamonds in Figure 9) form two clusters: the first is vertically elongated around the time of the maximum peak dose (between approximately 100,000 and 200,000 years); the second forms a curved streak, which is bounded by the black breakthrough curve associated with the realization that generated the maximum peak dose. The separation of the two clusters is a consequence of the non-symmetric influence of the two factors that have an impact on the peak dose time, namely the duration of the affinity effects (see Figure 6B) and the canister breach time (see Figure 3B). The first cluster is associated with realizations in which the influential factors affecting the peak dose—i.e., intrinsic and residual waste degradation rate, activation energy, and all the Υ factors—are combined with factors that lead to early peak dose times, which are left-skewed. The curved cluster is associated with realizations that lead to late peak dose times. Since a late arrival of radionuclides at the land surface is correlated to higher spatial and temporal dispersion of the contaminant plume, the peak dose values also decline with time at a rate that is consistent with that of the tail of the breakthrough curve with the maximum peak dose (black line). This suggests that the breakthrough curve with an *IRF* of 100% (see Figure 8B) not only defines the upper limit for the maximum peak dose, but it also provides bounds on peak dose

values for all combinations of source-term related parameter combinations.

Note that the uncertainty propagation analysis presented here is based on fairly large uncertainties and ranges in the input parameters (see Table 3), leading to a relatively large spread in the calculated peak dose values, which should be put in perspective to the spread caused by uncertainties in the conceptual models describing the thermal, hydrological, geochemical, mechanical, and biological processes and the large number of uncertain input parameters to the PA model. The contribution of the source-term model to prediction uncertainty is expected to be noticeable, but it may not dominate the conclusions of a comprehensive repository safety analysis.

4 Concluding remarks

The fundamental reason for disposing high-level radioactive waste in a geologic repository is the recognition that despite the encapsulation of the radionuclides in a solid waste form and its containment in a robust canister, these engineered barriers will eventually be breached, gradually releasing radionuclides into the near field of the repository. The key concern becomes the potential for these radionuclides to migrate to the accessible environment. Total system performance assessment calculations evaluate the effectiveness of the additional engineered barriers and specifically the geosphere to dilute the radionuclides through their slow release into the near field and retard their transport to the accessible environment. These long-term, post-closure performance assessments rely on a suitable and defensible model that describes the radiological source term used in the PA model. The insights gained here are relevant beyond any single repository concept, as they illustrate generalizable approaches to coupling waste-form degradation kinetics with multi-barrier performance models that can inform global waste management programs and regulatory evaluations.

Waste form degradation and radionuclide release depend on multiple, interacting factors, which are implemented in the source-term model by a combination of mechanistic process simulations, empirical correlations, and conservative assumptions. Despite the canister and waste form being engineered components of the repository system, determining their properties is difficult because the degradation processes are extraordinarily slow and affected by feedback mechanisms and conditions that change with time.

While canister corrosion and the dissolution and alteration of high level waste (HLW) glasses have been extensively studied, the impact of individual factors of the source-term model on the ultimate repository performance—here represented by the peak exposure dose—has not been systematically investigated. By integrating a rather comprehensive, suitably parameterized source-term model into an established simulator for coupled, non-isothermal fluid flow and radionuclide transport, we examined the link between individual source-term parameters—and their uncertainties—on peak dose. The following observations and conclusions can be made; they refer to a specific application of the proposed radiological source-term model to a generic vertical borehole repository.

- The release of radionuclides from a waste canister follows a complex, nonlinear function of multiple parameters describing waste degradation.
- For the reference scenario, which considers the disposal of 300 canisters with vitrified waste in a vertical borehole repository, the peak dose is approximately four orders of magnitude below a presumed dose standard of 0.1 mSv yr^{-1}. The predicted peak dose varies over approximately two orders of magnitude because of uncertainties in the source-term model parameters. The estimated time when peak dose occurs lies between 100,000 and 1,000,000 years.
- Multiple factors may have impacts on peak dose that are similar in magnitude. In particular, the intrinsic and residual degradation rates and the temporal evolution of affinity effects cause the largest deviation in peak dose if changed over their identified parameter range. Uncertainties in the predicted peak dose can be reduced if these factors (along with the activation energy, pH power-law exponent, and other composite factors describing the chemical environment) are determined as accurately as possible.
- In a vertical borehole repository, temperature effects on waste degradation are relevant due to the geothermal gradient. By contrast, the impact of repository-induced temperature changes on waste-form degradation is likely negligible if the canister is not breached until after the early portion of the thermal period.
- If a potential rate resumption is limited in magnitude (i.e., does not exceed the initial forward rate) or occurs after a prolonged period of waste degradation at the residual rate q_r, rate resumption is unlikely to lead to a dose that exceeds the primary peak value.
- Canister lifetime does not significantly impact peak dose for the specific repository design and reference conditions examined in this study. This conclusion applies to the case where total system performance is based on both the engineered and natural barrier systems. If site conditions or the repository concept do not warrant relying on the natural barrier system, and the waste form is prone to fast degradation leading to high radionuclide release rates, higher requirements for canister performance must be formulated.
- Simulating the instantaneous release of the entire radionuclide inventory provides a conservative bounding case, increasing peak dose by a factor of four over the reference scenario. This increase may be considered moderate in comparison to the range of uncertainties caused by factors that are not related to the source term. Furthermore, the breakthrough curve with an *IRF* of 100% also bounds the peak dose values for all combinations of source-term related parameter combinations.
- The waste form is a main component of the engineered barrier system, encapsulating radionuclides for an extended time and releasing them at very low rates which flatten the breakthrough curve by temporal and physical dilution.
- Studies on the radiological source term should focus on radionuclides that are relevant for the ultimate repository safety (i.e., peak exposure dose) rather than on the activity of a radionuclide as it is released from the canister.

In summary, this study shows that the source-term model and the uncertainties in its parameters influence the accuracy with which peak dose can be estimated. This means that both the conceptual model describing waste degradation and radionuclide release mechanisms must be carefully investigated for the given waste form. Moreover, key input parameters, such as the intrinsic and residual degradation rates, must be determined with high enough accuracy so they don't have an undue influence on PA model predictions.

If the current source-term model is considered an overly simplified representation of the processes that govern waste degradation and radionuclide release, it can be appropriately refined within the simulation framework presented here. Alternatively, more complex models, which mechanistically capture the coupled thermal, hydrological, and chemical processes, can be used (a) to validate the simplified model for its intended purpose within the context of a PA calculation, (b) to provide radionuclide release rates to the near field, or (c) directly in a high-fidelity PA model.

Data availability statement

The datasets presented in this article are not readily available because a scientific publication and data release is currently in preparation. Requests to access the datasets should be directed to jmclachlan@berkeley.edu.

Author contributions

SF: Conceptualization, Data curation, Formal Analysis, Methodology, Software, Validation, Visualization, Writing – original draft, Writing – review and editing. JM: Conceptualization, Data curation, Formal Analysis, Writing – review and editing. MH: Formal Analysis, Writing – review and editing. JS: Data curation, Project administration, Supervision, Writing – review and editing. RA: Conceptualization, Supervision, Writing – review and editing. PP: Conceptualization, Supervision, Writing – review and editing.

Funding

The author(s) declared that financial support was received for this work and/or its publication. The information, data, or work presented herein was funded in part by the Advanced Research Projects Agency-Energy (ARPA-E), U.S. Department of Energy, under Award Number DE-AR0001621. The views and opinions of authors expressed herein do not necessarily state or reflect those of the United States Government or any agency thereof.

Acknowledgements

We thank the two reviewers for their diligent reading of our manuscript as well as their pertinent comments and constructive suggestions.

Conflict of interest

Author SF was employed by Finsterle GeoConsulting, LLC. Author MH was employed by Hannon Clean Energy, LLC. Author JS was employed by Deep Isolation Nuclear, Inc.

The remaining author(s) declared that this work was conducted in the absence of any commercial or financial relationships that could be construed as a potential conflict of interest.

Generative AI statement

The author(s) declared that generative AI was not used in the creation of this manuscript.

Any alternative text (alt text) provided alongside figures in this article has been generated by Frontiers with the support of artificial intelligence and reasonable efforts have been made to ensure accuracy, including review by the authors wherever possible. If you identify any issues, please contact us.

Publisher's note

References

Achtziger-Zupančič, P., Loew, S., and Mariéthoz, G. (2017). A new global database to improve predictions of permeability distribution in crystalline rocks at site scale. *J. Geophys. Res. Solid Earth* 122, 3513–3539. doi:10.1002/2017JB014106

Andra (2016). *Dossier d'options de sûreté (DOS) du projet*. Châtenay-Malabry Cedex, France: Agence nationale pour la gestion des déchets radioactifs, 467. Report Cigéo. CG-TE-D-NTE-AMOA-SR2-0000-15-0062/A.

Caruso, S., Meleshyn, A., and Noseck, U. (2017). Estimation and comparison of the radionuclide inventories in vitrified high-level wastes from reprocessing plant. *Prog. Nucl. Energy* 94, 216–221. doi:10.1016/j.pnucene.2015.11.003

Cassingham, N., Corkhill, C. L., Backhouse, D. J., Hand, R. J., Ryan, J. V., Vienna, J. D., et al. (2015). The initial rates of simulated UK Magnox-ThORP blend nuclear waste glass as a function of pH, temperature and waste loading. *Mineral. Mag.* 79 (6), 1529–1542. doi:10.1180/minmag.2015.079.6.28

Crawford, C. L., Marra, J. C., and Bibler, N. E. (2007). Glass fabrication and product consistency testing of lanthanide borosilicate glass for plutonium disposition. *J. Alloys Compd.* 444–445, 569–579. doi:10.1016/j.jallcom.2007.02.164

Curti, E. (2022). *Aqueous corrosion of vitrified nuclear waste: current process understanding, literature review and recommended rates*. Nagra Arbeitsbericht NAB 23-09. Wettingen, Switzerland: National Cooperative for the Disposal of Radioactive Waste. Available online at: https://nagra.ch/en/downloads/arbeitsbericht-nab-23-09-3/.

Curti, E., Crovisier, J. L., Morvan, G., and Karpoff, A. M. (2006). Long-term corrosion of two nuclear waste reference glasses (MW and SON68): a kinetic and mineral alteration study. *Appl. Geochem.* 21 (7), 1152–1168. doi:10.1016/j.apgeochem.2006.03.010

De Echave, T. (2018). *Etude des mécanismes d'altération des verres nucléaires sous radiolyse alpha et en conditions environnementales*. Montpellier, France: Université Montpellier. Dissertation.

Deissmann, G., Neeft, E., and Jacques, D. (2025). EURAD state-of-the-astate-of-the-art report: assessment of engineered materials and natural analogues for degradation in disposal environments. *Front. Nucl. Eng.* 3, 1433257. doi:10.3389/fnuen.2024.1433257

Ebert, W. L. (2006). *Corrosion testing of a plutonium-loaded lanthanide borosilicate glass made with frit B*. Report ANL-06/35, 925325. doi:10.2172/925325

Finsterle, S. (2015). Practical notes on local data-worth analysis. *Water Resour. Res.* 51 (12), 9904–9924. doi:10.1002/2015WR017445

Finsterle, S. (2025). *Enhancements to the TOUGH2 simulator integrated in iTOUGH2, report FGC-18-02/LBNL-7016E*. Kensington, CA, United States: Finsterle GeoConsulting, LLC. Available online at: https://www.finsterle-geoconsulting.com/s/TOUGH2-In-iTOUGH2_Enhancements.pdf.

Finsterle, S., Commer, M., Edmiston, J., Jung, Y., Kowalsky, M. B., Pau, G. S. H., et al. (2017). iTOUGH2: a simulation-optimization framework for analyzing multiphysics subsurface systems. *Comput. and Geosciences* 108, 8–20. doi:10.1016/j.cageo.2016.09.005

Finsterle, S., Muller, R. A., Baltzer, R., Payer, J., and Rector, J. W. (2019). Thermal evolution near heat-generating nuclear waste canisters disposed in horizontal drillholes. *Energies* 12 (4), 596. doi:10.3390/en12040596

Finsterle, S., Muller, R. A., Grimsich, J., Apps, J., and Baltzer, R. (2020). Post-closure safety calculations for the disposal of spent nuclear fuel in a generic horizontal drillhole repository. *Energies* 13, 2599. doi:10.3390/en13102599

Finsterle, S., Cooper, C., Muller, R. A., and Apps, J. (2021a). Sealing of a deep horizontal borehole repository for nuclear waste. *Energies* 14 (1), 91. doi:10.3390/en14010091

Finsterle, S., Muller, R. A., Grimsich, J., Bates, E. A., and Midgley, J. (2021b). Post-closure safety analysis of nuclear waste disposal in deep vertical boreholes. *Energies* 14 (19), 6356. doi:10.3390/en14196356

Finsterle, S., Waples, M., Yang, M., and Travis, K. P. (2025). Generation and dissipation of corrosion gas in a deep horizontal borehole repository for radioactive waste. *Front. Nucl. Eng.* 4 (4), 1689795. doi:10.3389/fnuen.2025.1689795

Fournier, M., Gin, S., and Frugier, P. (2014). Resumption of nuclear glass alteration: state of the art. *J. Nucl. Mater.* 448 (1–3), 348–363. doi:10.1016/j.jnucmat.2014.02.022

Fournier, M., Frugier, P., and Gin, S. (2018). Application of GRAAL model to the resumption of international simple glass alteration. *Npj Mater. Degrad.* 2 (21), 21. doi:10.1038/s41529-018-0043-4

Gin, S., Jollivet, P., Tribet, M., Peuget, S., and Schuller, S. (2017). Radionuclides containment in nuclear glasses: an overview. *Radiochim. Acta* 105 (11), 927–959. doi:10.1515/ract-2016-2658

Harper, C. O., Brown, J. L., and Amos, R. T. (2024). Corrosion processes affecting copper-coated used fuel containers for the disposal of spent nuclear fuel: critical review of the state-of-knowledge. *Npj Mater. Degrad.* 8 (124), 124. doi:10.1038/s41529-024-00540-z

IAEA (2003). *Reference biospheres for solid radioactive waste disposal*. Vienna, Austria: International Atomic Energy Agency, 560. Report IAEA-BIOMASS-6.

IAEA (2011). *Disposal of radioactive waste*. Vienna, Austria: International Atomic Energy Agency, 560. IAEA Safety Standards Series No. SSR-5.

Jantzen, C. M. (2011). "Development of glass matrices for high level radioactive wastes," in *Handbook of advanced radioactive waste conditioning technologies*. Editor M. I. Ojovan (Sawston, Cambridge, United Kingdom: Woodhead Publishing Series in Energy, Woodhead Publishing), 230–292. doi:10.1533/9780857090959.2.230

Johnson, L. H., Curti, E., and Spahiu, K. (2023). *A radionucldie rleease model for spent UO_2 and MOX fuel for safety assessment with application to waste to be disposed of in a deep geological repository in Switzerland*. Wettingen, Switzerland: National Cooperative for the Disposal of Radioactive Waste. Nagra Arbeitsbericht NAB 23-10.

Jones, T. (2006). *Glass macrocracking determination in prototypic canisters containing lanthanide borosilicate glass*. Aiken, SC: Savannah River National Laboratory. Report WSRC-TR-2006-00015. doi:10.2172/882729

Kessler, J. L. (2002). *Effect of cooling rate, thermal expansion, and waste loading on glass fracture*. Aiken, SC, United States: Savannah River Laboratory. Memorandum DPST-82-490. doi:10.2172/804679

Kienzler, B., Altmaier, M., Bube, C., and Metz, V. (2012). *Radionuclide source term for HLW glass, spent nuclear fuel, and compacted hulls and end pieces (CSD-C waste)*. Karlsruhe, Germany: Karlsruher Institut für Technologie. Report KIT-SR 7624.

King, F., Kolàr, M., Briggs, S., Behazin, M., Keech, P., and Diomidis, N. (2024). Review of the modelling of corrosion processes and lifetime prediction for HLW/SF containers—Part 2: performance assessment models. *Corros. Mater. Degrad.* 5 (2), 289–339. doi:10.3390/cmd5020013

Marcial, J., Chesnutt, J., Neeway, J. J., Gichon, E., Thorpe, C. L., Zhu, Z., et al. (2025). Alteration of archeological and natural analogs for radioactive waste glass under different environmental conditions. *Npj Mater Degrad.* 9 (102), 102. doi:10.1038/s41529-025-00624-4

Marra, J. E. (2006). *Glass fabrication and product consistency testing of lanthanide borosilicate frit B composition for plutonium disposition*. Aiken, SC, United States: Westinghouse Savannah River Company/Savannah River Technology Center. Report WSRC-TR-2006-00033.

Marra, J. E., and Ebert, W. (2003). *Accounting for a vitrified plutonium waste form in the Yucca Mountain repository total System Performance assessment (TSPA)*. Aiken, SC, United States: Westinghouse Savannah River Company/Savannah River Technology Center. Report WSRC-TR-2003-00530. doi:10.2172/901094

McCloy, J. S., Riley, B. J., Dixon Wilkins, M. C., Evarts, J. S., Bussey, J., Vienna, J. D., et al. (2024). International perspectives on glass waste form development and durability. *Mater. Today* 80, 594–618. doi:10.1016/j.mattod.2024.08.025

McLachlan, J. R., Wang, T.-C., Chui, R., Tang, S. Z., Scarlat, R. O., Peterson, P. F., et al. (2024). *Lanthanide borosilicate glasses: literature summary, experimental results, and performance assessment recommendations*. Berkeley, CA, United States: Deep Isolation, Inc. Report ARPA-E: UPWARDS Milestone 1.3.

Mougnaud, S., Tribet, M., Renault, J.-P., Jollivet, P., Panczer, G., Charpentier, Y., et al. (2016). Effect of low dose electron beam irradiation on the alteration layer formed during nuclear glass leaching. *J. Nucl. Mater.* 482, 53–62. doi:10.1016/j.jnucmat.2016.10.008

Mougnaud, S., Tribet, M., Renault, J.-P., Gin, S., Peuget, S., Podor, R., et al. (2018). Heavy ion radiation ageing impact on long-term glass alteration behavior. *J. Nucl. Mater.* 510, 168–177. doi:10.1016/j.jnucmat.2018.07.046

Muller, R. A., Finsterle, S., Grimsich, J., Baltzer, R., Muller, E. A., Rector, J. W., et al. (2019). Disposal of high-level nuclear waste in deep horizontal drillholes. *Energies* 12, 2052. doi:10.3390/en12112052

Muñoz, A. G., Abdelouas, A., Alonso, U., Fernández, A. M., Bernier-Latmani, R., Cherkouk, A., et al. (2024). WP15 ConCorD state-of-the-art report (container corrosion and degradation in repository conditions). *Front. Nucl. Eng.* 3. doi:10.3389/fnuen.2024.1404739

Nagra (1994). *Kristallin-I—Safety assessment report*. Wettingen, Switzerland: National Cooperative for the Disposal of Radioactive Waste. Nagra Technical Report NTB 93-22.

Nagra (2014a). *Provisional safety analyses for SGT stage 2—Models, codes, and general modelling approach*. Wettingen, Switzerland: National Cooperative for the Disposal of Radioactive Waste. Nagra Technical Report NTB 14-09.

Nagra (2014b). *Safety case for the disposal of high-level waste and spent fuel in a geological repository in the opalinus clay of northern Switzerland (project opalinus clay)*. Wettingen, Switzerland: National Cooperative for the Disposal of Radioactive Waste. Nagra Technical Report NTB 14-01.

Nagra (2024). *Radiological consequence analysis for a deep repository in northern Switzerland*. Wettingen, Switzerland: National Cooperative for the Disposal of Radioactive Waste. Nagra Technical Report NTB 24-18.

NRC (2014). *Safety evaluation report related to the U.S. department of energy's license application for a geologic repository at Yucca Mountain*. Washington, DC: United States Nuclear Regulatory Commission. Report NUREG-1049.

Peeler, D. K., Edwards, T. B., Rudisill, T. S., Reamer, I. A., Vienna, J. D., Smith, D. E., et al. (1999). *Composition/property relationships for the phase 2 Am/Cm glass variability study (U)*. Aiken, SC: Westinghouse Savannah River Company/Savannah River Technology Center. WSRC-TR-99-00393. doi:10.2172/756601

Peters, R., and Slate, S. (1982). Fracturing of simulated high-level waste glass in canisters. *Nucl. Eng. Des.* 67 (3), 425–445. doi:10.1016/0029-5493(82)90071-1

Pruess, K., Oldenburg, C., and Moridis, G. (2012). *TOUGH2 User's Guide, Version 2.1*. Berkeley, CA: Lawrence Berkeley National Laboratory Report LBNL-43134.

Ramsey, W. G., Bibler, N. E., and Meaker, T. F. (1995). *Compositions and durabilities of glasses for immobilization of plutonium and uranium*. Aiken, SC, United States: Westinghouse Savannah River Company/Savannah River Technology Center. WSRC-MS-94-0550; CONF-950216-142. doi:10.2172/63953

SKB (2005). *The effect of dissolved hydrogen on the sissolution of ^{233}U doped UO_2 (s), high Burn-up spent fuel and MOX fuel*. Stockholm, Sweden: Svensk Kärnbränslehantering AB. Report TR-05-09.

SKB (2011). *Long-term safety for the final repository for spent nuclear fuel at forsmark*. Stockholm, Sweden: Svensk Kärnbränslehantering AB. Report TR-11-01.

Thorpe, C. L., Neeway, J. J., Pearce, C. I., Hand, R. J., Fisher, A. J., Walling, S. A., et al. (2021). Forty years of durability assessment of nuclear waste glass by standard methods. *Npj Mater. Degrad.* 5 (61), 61. doi:10.1038/s41529-021-00210-4

Tribet, M., Marques, C., Mougnaud, S., Broudic, V., Jegou, C., and Peuget, S. (2021). Alpha dose rate and decay dose impacts on the long-term alteration of HLW nuclear glasses. *npj Materials Degradation* 5 (1), 36.

Vienna, J. D., Neeway, J. J., Ryan, J. V., and Kerisit, S. N. (2018). Impacts of glass composition, pH, and temperature on glass forward dissolution rate. *Npj Mater. Degrad.* 2 (22), 22. doi:10.1038/s41529-018-0042-5

Zhang, Y., and Pinder, G. (2003). Latin hypercube lattice sample selection strategy for correlated random hydraulic conductivity fields. *Water Resour. Res.* 38 (8), 1226. doi:10.1029/2002WR001822